The theory of free inertial jets

II. *A numerical experiment for the path of the Gulf Stream*

By P. P. NIILER[1] and A. R. ROBINSON, *Pierce Hall, Harvard University*

(Manuscript received January 13, 1967)

ABSTRACT

Numerical solutions are obtained to the path equation of the free jet which was derived in Part I of this study, for values of the parameters relevant to the Gulf Stream. Comparison is made with the observational data. It is shown that this steady state theory can describe the mean position of the stream as it falls off the continental shelf into deep water. The meandering of the stream about this mean position is discussed in some detail.

1. The model

1.1. *Introduction*

An outline of a complete theory of free inertial currents has been presented as Part I of this study (Robinson & Niiler, 1967). Here this steady state theory for the path of such a current is applied in the region of the North Atlantic from Cape Hatteras east to the Grand Banks and north to the continental shelf, and comparison is made with the available observational data on the Gulf Stream. This is accomplished by the numerical integration of the equation for the path over a wide range of determinative conditions, restricted only to be at least remotely consistent with the observational data and not to contradict grossly the assumption made in the derivation of the equation.

1.2. *The equation*

A free current, whose downstream velocity component is almost geostrophic has a cross-stream pressure gradient which is much larger than that characteristic of the open ocean on either side of the current. The diminution of this pressure gradient on the edges of the current is effected necessarily by the distributions of mass and sea-level. This relates features of the structure of the current to its path, which may be formally seen in the consequences of an integration of the equation for the vertical component of vorticity over the cross-sectional plane normal to the axis of the current. The result is (vid. Part I, eq. (2.31))

$$\int_{-\infty}^{+\infty} dx \left\{ \int_{B(y)}^{H} dz \left[\frac{\partial}{\partial y}(\varkappa v^2) + v \frac{\partial \beta}{\partial y} \right] + f v(B) \frac{\partial \beta}{\partial y} \right\} = 0, \tag{1.1}$$

where use has been made of mass continuity and of the bottom boundary condition of vanishing normal velocity. Here (x, y) are local cross-stream and downstream axis coordinates, z is vertical, $\pm\infty$ represent the right and left hand edges of the current, and $v(B) \equiv v(x, y, B(y))$. The current has been assumed to be narrow, so that the Coriolis parameter ($f = f_0 + \beta(y)$), the deviation of the bottom from the mean depth $z = 0$ ($B(y)$) and the local curvature ($\varkappa(y)$), are taken to depend only on the downstream distance.

In terms of the geographical coordinates X, Y (eastward and northward), $f = f_0 + \beta_0 Y$, $B(X, Y)$ is a known function, and $\varkappa = d^2Y/dX^2\ (1 + (dY/dX)^2)^{-\frac{3}{2}}$ along any curve $Y(X)$. Thus if the requisite integral properties of the current velocity were known, eq. (1.1) would provide an integro-differential equation for the current path. The circumstances under which eq. (1.1) provides an approximate differential equation for the path were discussed in Part I, § 5. Briefly, if the bottom variations are small compared to the mean depth and if the north-south excursion of the stream is not large (which

[1] Now at Nova University, Fort Lauderdale, Florida.

imply that the radius of curvature of the meanders is smaller than the width of the current), then it is correct to evaluate the vertical integrals over the mean depth and to ignore the structural changes in the velocity which necessarily accompany meandering. It is consistent, however, to allow slow changes in the current velocity which represent, e.g., a gain or loss of transport or bottom velocity which is insignificant over a single meander but significant over many. Such a change in the stream structure here parameterizes the general circulation of the basin; i.e., the stream may lose mass to the open ocean region. The slow downstream change of the velocity profile will be referred to as divergence (or convergence) of the stream.

It is convenient to integrate eq. (1.1) by parts in y. There results, under the approximations mentioned above,

$$\varkappa\langle v^2\rangle - \varkappa(0)\langle v_0^2\rangle + f_0\bar{v}(B-B_0) + \langle v\rangle\beta - f\int_0^y (B-B_0)\frac{d\bar{v}}{dy^*}dy^* - \int_0^y \beta\frac{d\langle v\rangle}{dy^*}dy^* = 0, \tag{1.2 a}$$

where

$$\langle v^2\rangle \equiv \int_0^H dz\int_{-\infty}^{\infty} dx v^2(x,y,z),$$

$$\langle v\rangle \equiv \int_0^H dz\int_{-\infty}^{\infty} dx v(x,y,z),$$

$$\bar{v} \equiv \int_{-\infty}^{\infty} dx v(x,y,B(y)), \tag{1.2 b}$$

and a 0-subscript refers to $y=0$.

The effect of divergence will be treated simply by allowing the integral properties, which appear in the coefficients, to be linear functions of the path length. This follows naturally from the downstream expansion introduced in Part I § 5.2. In this part, however, the problem of the structure of the current will be suppressed, i.e. simple model profiles and divergence rates will be assumed. The model profiles will be specified by a discrete set of parameters, in terms of which the downstream rates of change of the integrals (1.2a) will be related.

The standard form of (1.2a) adopted for integration and discussion is then

$$(1+\varepsilon_0 y)\varkappa - C_0 + C_1\left[(1+\varepsilon_1 y)(B-B_0) - \varepsilon_1\int_0^y (B-B_0)dy^*\right] + C_2\left[(1+\varepsilon_2 y)(Y-Y_0) - \varepsilon_2\int_0^y (Y-Y_0)dy^*\right] = 0, \tag{1.3}$$

where $$dy = \left(1+\left(\frac{dY}{dX}\right)^2\right)^{\frac{1}{2}} dX.$$

The (dimensional) constants are defined by

$$C_0 \equiv 10^6\varkappa(0),\quad C_1 \equiv \frac{10^{10} f_0 \bar{v}_0}{\langle v_0^2\rangle},\quad C_2 \equiv \frac{10^{12}\beta_0\langle v\rangle}{\langle v_0^2\rangle} \tag{1.4 a}$$

and

$$\varepsilon_0 y \equiv \frac{\langle v^2\rangle}{\langle v_0^2\rangle} - 1,\quad \varepsilon_1 y \equiv \frac{\bar{v}}{\bar{v}_0} - 1,\quad \varepsilon_2 y \equiv \frac{\langle v\rangle}{\langle v_0\rangle} - 1, \tag{1.4 b}$$

with the path length y and Y measured in a linear unit of 10 km and B in units of 100 m. An alternative definition of 0_1, and the definition of an additional parameter which does not appear in eq. (1.3), but which will be useful in the discussion of the dependence of the constants on assumed velocity profiles, are

$$\varepsilon_1 y = \frac{v(0,y,0)}{v(0,0,0)} - 1,\quad \varepsilon_3 y = \frac{v(0,y,H)}{v(0,0,H)} - 1, \tag{1.5}$$

The dependence of the path solutions upon a wide range of values of C_i, ε_i is investigated in section 2; in section 3, C_i, ε_i are related to the maximum surface and bottom velocities of various models of the stream. In section 4 the behavior of the real Gulf Stream is discussed and in section 5 the solution paths pertinent to the Gulf Stream are developed and compared to the observations.

1.3. *Numerical procdure for integrating the path equation*

The integration of the path equation (1.3) begins by specifying a $Y(0)$, $Y'(0)$. A maximum integration step is chosen (here 17.1 km) and

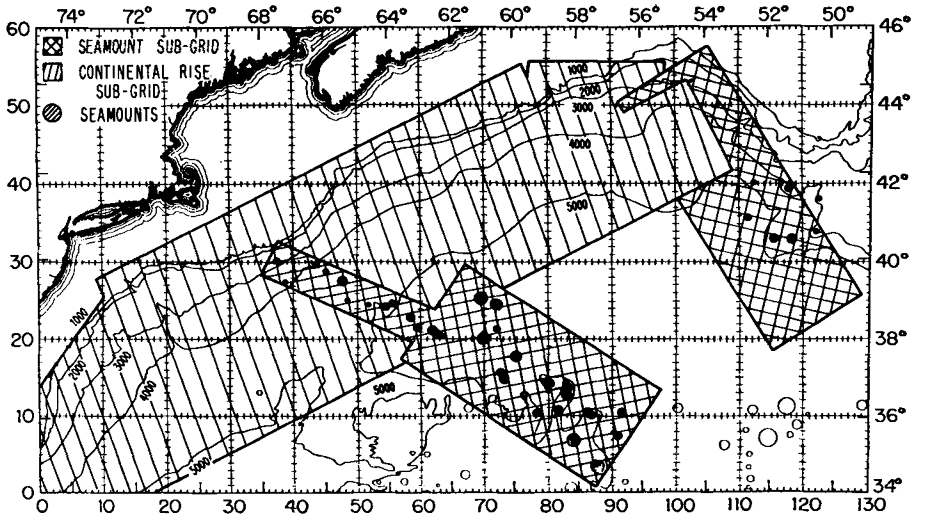

Fig. 1. Deep-sea topography off the east coast of the United States with superimposed integration grid and sub-grids.

the values of $Y_{1\text{-step}}$, $Y'_{1\text{-step}}$ are obtained at the new point by the Runge–Kutta method of forward interpolation. The integration step size is then halved, and the procedure is repeated twice in line, whereby a $Y_{2\text{-step}}$, $Y'_{2\text{-step}}$ at the 1-step integration point is obtained. If the difference between the 1-step and 2-step solutions is less than a standard maximum error, the procedure is considered convergent and is continued forward with a maximum step size. If the difference is more than a standard maximum error, the 1-step integration step is halved until the process becomes convergent. If at any integration step, the difference between the 1-step and 2-step solutions is less than a minimum standard error, the next 1-step integration step is doubled. This procedure continues until either the solution path runs off the integration grid, or the step size becomes less than the maximum standard error.

The Runge–Kutta method of integration in X, Y coordinates is useful if Y', Y'' remain finite. Hence, if both $Y' > 1$ and $Y'' > 10$, the integration grid is rotated 90°. The convergent integration step before rotation provides the initial conditions for the integrating procedure in the rotated system. The rotated version of (1.3) is the equation to be solved in the rotated coordinate system.

The value of $B(X, Y)$ used in (1.3) is an averaged bottom depth value. The deep-sea topography map compiled by Pratt (1965) was used to obtain the actual depth at any given longitude and latitude. Nine separate sub-grids (see Fig. 1) were superimposed on Pratt's map, and the depth was recorded at each grid point. Two sub-grids contained the majority of the Bermuda–New England sea mount arc and the remainder were arranged parallel to the prevailing contours at a region. To find the value of the actual depth at the positions between sub-grid points, a polynomial interpolating scheme was adopted. A one degree polynomial interpolation was used in the direction along the contours and a third degree polynomial interpolation was adopted in the direction across the contours. In the sea-mount regions and abyssal plain area, the interpolation was linear in both directions. The radius of the region of influence of an interpolated value varied from 6.5 km to 115 km. The average value of the depth used in (1.3) was computed from $B(X, Y) = \frac{1}{2}\ [\mathcal{B}(X, Y) + \frac{1}{2}[\mathcal{B}^-(X, Y) + \mathcal{B}^+(X, Y)]]$, where $\mathcal{B}$ is the actual interpolated value of the bottom at the solution X, Y, and $\mathcal{B}^+$ and $\mathcal{B}^-$ are the values 25 km in either direction normal to the solution path. In (1.3) the integrals are computed as the sum of trapezoidal sections which are bounded laterally by values of the integral at convergent solution points and separated by the integration step size.

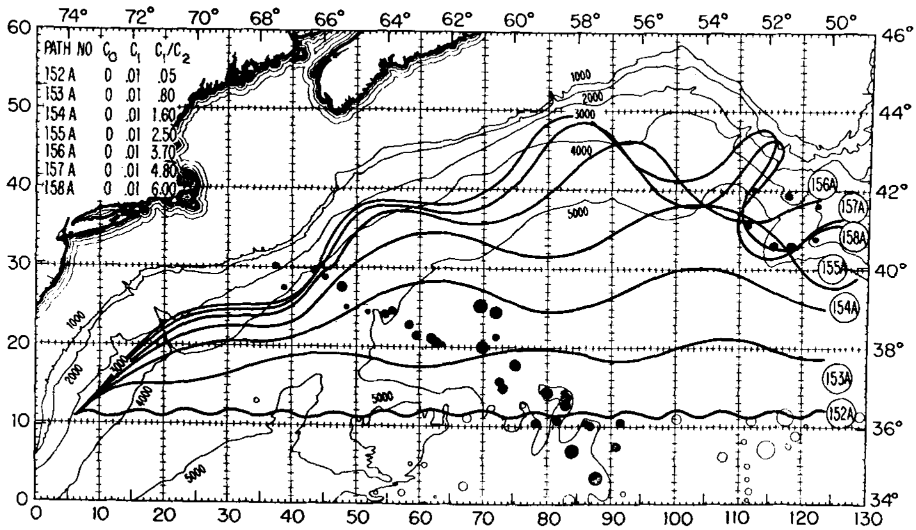

Fig. 2. Effect of variation of C_1/C_2 for fixed C_1 (vid. eq. 1.4*a*).

2. Solution of the path equation

2.1. *Analytic development of the control curve*

The collection of points of the solutions of (1.3), with fixed C_i, ε_i, where curvature is zero, can in most instances be simply connected to form a smooth curve. The solution paths of (1.3) which are physical (non-eddying) meander about this control curve. The control curve simply maps out the mean position of the stream.

Set $\varkappa = 0$ in (1.3), whereby the control curve $\mathcal{Y}_0(X)$ is determined from

$$-C_0 + C_1(1+\varepsilon_1\eta_0)[B(X,\mathcal{Y}) - B_0] + C_2(1+\varepsilon_2\eta_0)(\mathcal{Y} - Y_0) = C_1\varepsilon_1\int_0^{\eta_0}(B-B_0)\,d\eta_0 + C_2\varepsilon_2\int_0^{\eta_0}(\mathcal{Y}-Y_0)\,d\eta_0, \tag{2.1}$$

$$\eta_0 = \int_0^X (1+\mathcal{Y}'^2)^{\frac{1}{2}}\,dX. \tag{2.2}$$

In the above η_0 is the length of the control curve. Strictly, the integration should be along the arc length of the solution curve η. Since η is a monotonic function of η_0, replacing η by η_0 in (2.1) effectively changes the value of ε of the solutions of (1.3), which oscillate about the control curve determined by (2.1), (2.2). In the case $\varepsilon = 0$, no such ambiguity in interpretation arises.

The quantity $\varepsilon\eta_0 < 1$ for it parametrizes small divergence along the control curve. A power series solution in this quantity is obtained for $\mathcal{Y}$. Set $\varepsilon\eta_0 = 0$ in (2.1) whereby

$$-C_0 + C_1(B - B_0) + C_2(\mathcal{Y}^{(0)} - Y_0) = 0. \tag{2.3}$$

Divergence causes an additional displacement

$$\mathcal{Y}^{(1)}[C_1 B_Y(X,\mathcal{Y}^{(0)}(X)) + C_2] = C_2[\varepsilon_1 - \varepsilon_2] \times \left[\eta_0\mathcal{Y}^{(0)} - \int_0^{\eta_0}\mathcal{Y}^{(0)}\,d\eta_0\right]. \tag{2.4}$$

Consider the simplest case of (2.3), (2.4), $C_2 = C_0 = \varepsilon_i = 0$. In this case the control curve is the isobath on which the stream begins its sinuous path with zero curvature. For $C_0 \neq 0$, but $C_2 = \varepsilon_i = 0$, the control curve is again an isobath at a depth proportional to (C_0/C_1) from the initial isobath. If $C_2 \neq 0$, but $\varepsilon_i = C_0 = 0$, the control curve leaves the isobath at a rate which is a function of (C_1/C_2).

Meandering about the control curve can be caused by various mechanisms (vid. Part I § 3.1). If $C_0 = \varepsilon = 0$, the meandering is a result of slowly curving isobaths or a result of pointing the stream initially at an angle to the control curve. The equation for small amplitude oscillations about the slowly curving control curve is

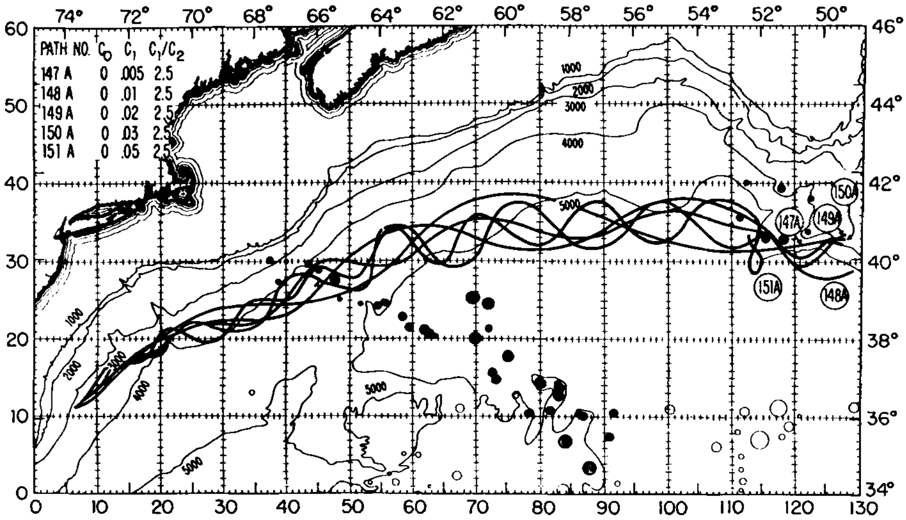

Fig. 3. Effect of variation of C_1 for fixed C_1/C_2 (vid. eq. 1.4*a*).

$$\frac{d^2Y_1}{dX^2} + [1+\mathcal{Y}'^2]^{\frac{3}{2}}[C_1 B_Y(X, \mathcal{Y}(X)) + C_2]\,Y_1 = -\frac{d^2\mathcal{Y}}{dX^2}. \tag{2.5}$$

It is seen from (2.5) that oscillations about the control curve have a local half-wavelength $\pi\{(1+\mathcal{Y}'^2)^{\frac{3}{2}}\ [C_1 BY\ (X,\mathcal{Y})+C_2]\}^{-\frac{1}{2}}$. A non-zero value of C_0 also causes meandering about the control curve, a phenomena not readily isolable analytically.

2.2. *Non-divergent stream paths over North Atlantic topography*

(a) *Effect of* C_0, C_1, C_2. The values of C_0, C_1, C_2, for which numerical integration of (1.3) has been carried out over the North Atlantic topography, are chosen to lay in the neighbourhood of the values pertinent to the observed Gulf Stream (vid. section 3). Recall from the previous section that the ratio (C_1/C_2) determines the control curve and mean location of the stream path. Figure 2 displays a collection of stream paths for $C_1 = 0.1$ and various values of (C_1/C_2).

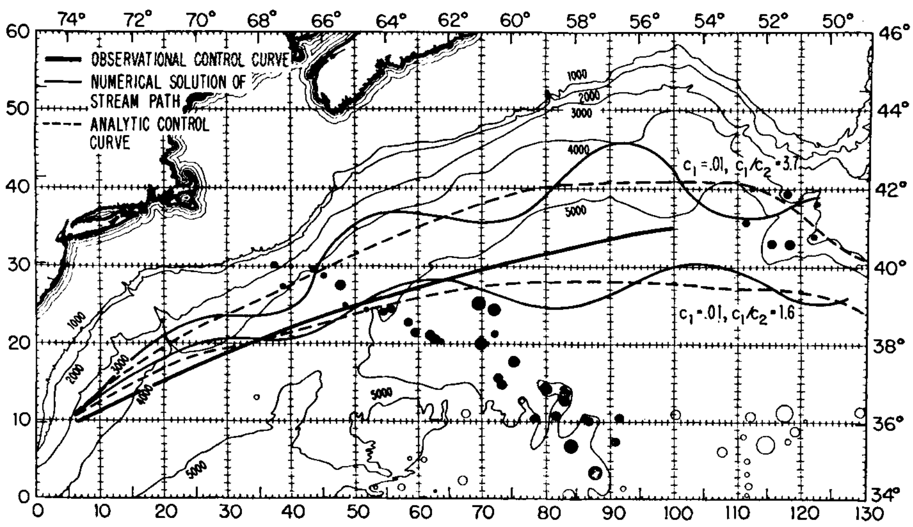

Fig. 4. Control curves of solution paths.

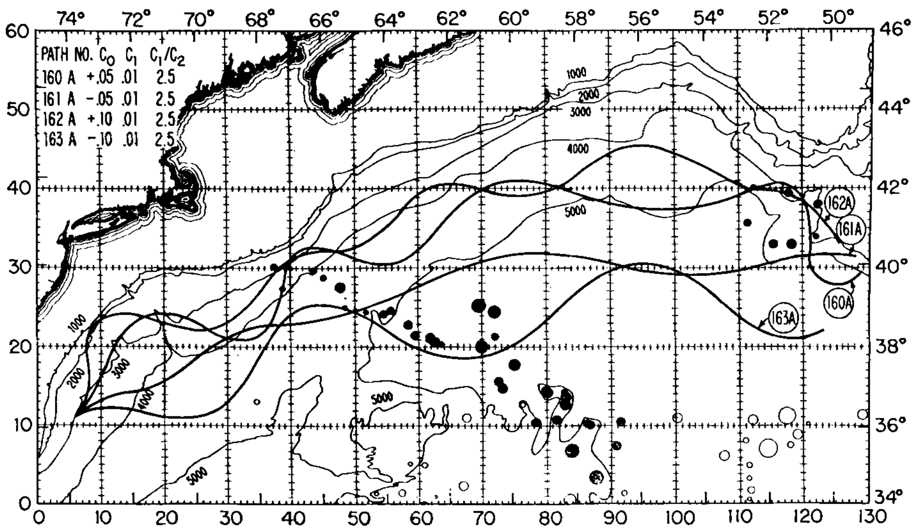

Fig. 5. Effect of variation of C_0 with fixed C_1, C_1/C_2 (vid. eq. 1.4a).

For large values of this parameter the path is controlled by topographic features, meandering about the initial isobath; for small values it is a Rossby wave, meandering about the initial latitude circle. For fixed (C_1/C_2), the local wavelength is proportional to $C_1^{-\frac{1}{2}}$. Figure 3 displays a class of solutions for fixed $(C_1/C_2) = 2.5$, and various values of C_1. Note that from solution path 147A to 149A, C_1 is increased by a factor of 4, while the wavelength decreases only by a factor of 2. Solution paths are plotted on Figure 4 along with analytic control curves corresponding to these paths. The calculated mean wavelength from the above analytical considerations for these paths is 359 km; the actual mean wavelength is 332 km.

The effect of varying C_0 is displayed in Figure 5. Positive C_0 forces the mean position of the stream into steeply sloping shallows. Note that as the bottom slope steepens, the effective C_1 increases and the meanders shorten. Negative C_0 for the North Atlantic has the reverse effect. If C_0 is increased (to >0.2), the large initial curvature constrains the path to become circular.

(b) *Effect of bathymetry detail, initial location and direction.* It was found that, in the range of C_0, C_1, C_2 relevant to he Gulf Stream, the solution paths were insensitive to the fine scale details (changes of 100 m in 50 km) of the North Atlantic bathymetry. Solution paths were obtained with randomized bathymetry values, i.e., at each step of integration a random depth between $\pm$ 100 m was added to the interpolated averaged depth (vid. section 1). Besides using an interpolated averaged depth in the integrating procedure, the actual interpolated depth at a solution point was used in obtaining solution paths. In both instances, less than 1 % difference in the solution with identical C_i, $Y'(0)$, $Y(0)$ resulted.

The effects of changing the initial location and direction of the stream are displayed in Figure 6 and 7. A change of initial location changes the control curve to a different isobath. If the initial isobaths are close together and remain so, the solution paths also remain close together. The larger the initial angle the solution path makes with the control curve, the larger the (meandering) amplitude is about the control curve. Recall from Part I of this study that increasing amplitude reduces the wavelength and finally eddying results.

2.3. *Divergent tendencies over a uniformly sloping bottom*

The equation of the stream path over uniformly sloping bottom is (vid. Part I, eq. (3.18))

$$\varkappa[1+\varepsilon_0 y] - \varkappa_0 + [1+\varepsilon_1 y]\, Y = \varepsilon_1 \int_0^y Y dy, \qquad (2.6)$$

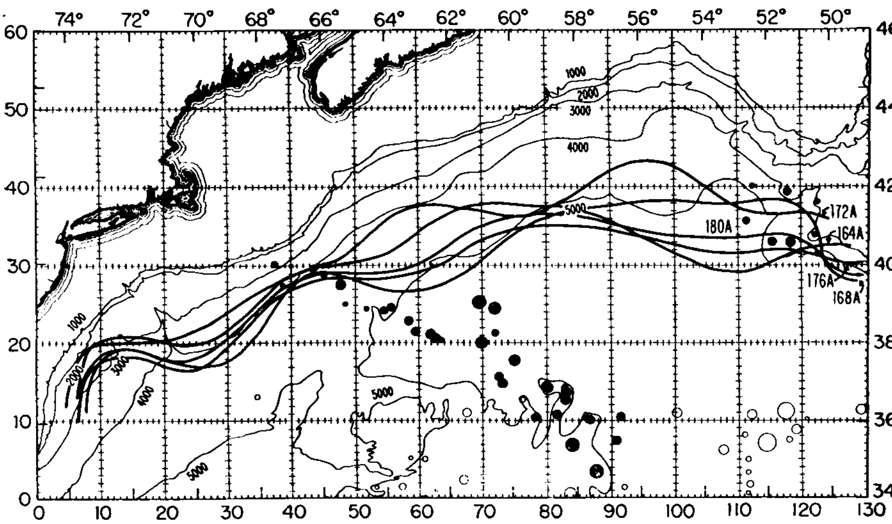

Fig. 6. Effect of varying initial location of an initially northward pointing stream. $C_0=0$, $C_1=0.01$, $C_1/C_2=2.5$.

$$y=\int_0^X [1+Y'^2]^{\frac{1}{2}}dX. \qquad (2.7)$$

The solutions of (2.6) with $\varepsilon_0=\varepsilon_1=0$ have been investigated in Part I of this study, and are a guide to the behaviour of the solutions over the complex real topography. Here the effect of small divergence, $\varepsilon_0 y$, $\varepsilon_1 y<1$, has been considered. Figures 8 and 9 display a wide class of these solutions. Divergence tends to make the stream more baroclinic if the bottom velocity decreases faster than the top velocity, more barotropic if the bottom velocity decreases slower than the top velocity. The results of this numerical analysis are summarized in Table 1.

At a fixed longitude X, the effect of a $\varkappa_0$ or increasing the initial slope enhances the divergent effects.

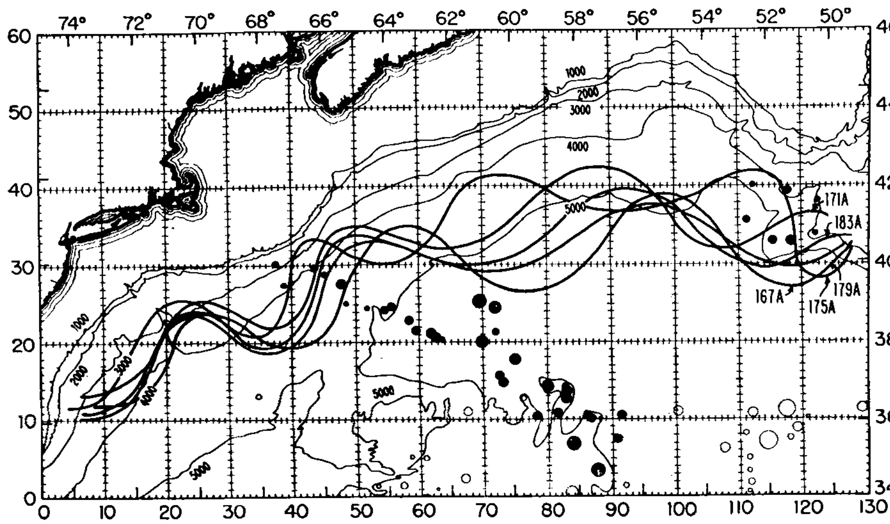

Fig. 7. Effect of varying initial location of an initially eastward pointing stream. $C_0=0$, $C_1=0.01$, $C_1/C_2=2.5$.

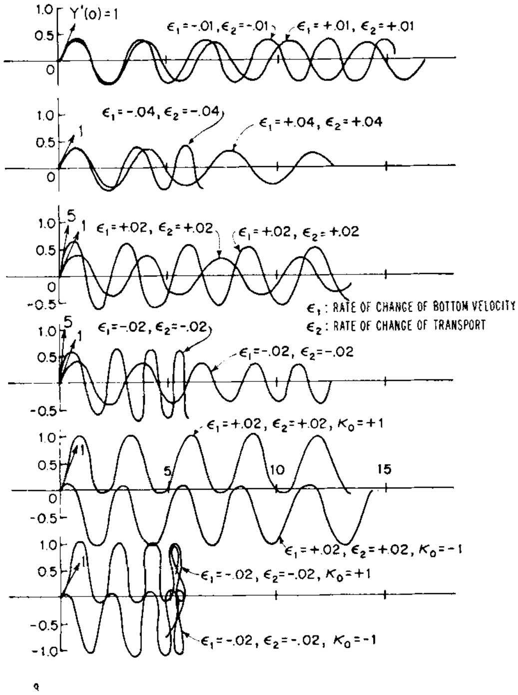

Fig. 8. Divergent-convergent stream paths over uniformly sloping bottom.

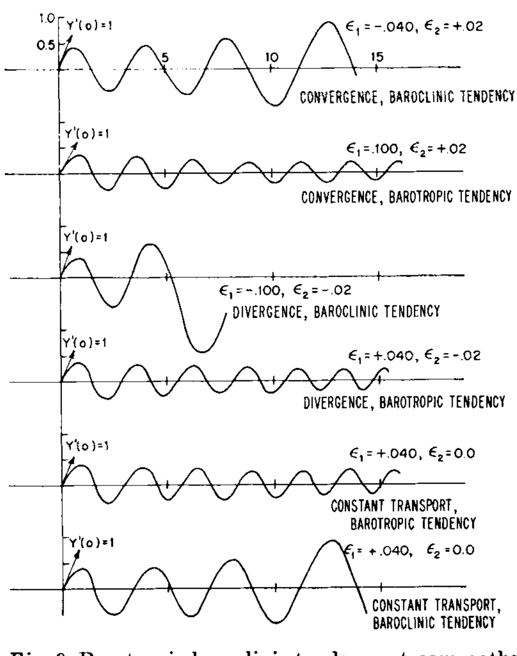

Fig. 9. Barotropic-baroclinic tendency stream paths over uniformly sloping bottom.

Table 1. *Summary of divergent effects on meander amplitude and wavelength as compared with non-divergent stream paths*

A plus sign indicates an increase of the associated property etc.

	Amplitude	Wavelength
Divergence	+	−
Convergence	−	+
Baroclinic tendency	−	−
Barotropic tendency	+	+

2.4. *Divergent stream paths over North Atlantic topography*

Figure 10 summarizes the effect of divergence on a typical stream path in the North Atlantic basin. In terms of an exponential velocity structure model of the stream (vid. section 4), the percentage changes of the average stream properties over the path length are summarized in Table 2. Figure 24 interprets these divergent paths on a top velocity and bottom velocity grid diagram.

3. Dependence of C_1 and C_2 on the structure of the stream

3.1. *The exponential model*

The numerical values of the constant C_1, C_2, ε_0, ε_1, ε_2 depend upon the axial velocity structure of the stream. Here the values of these constants are calculated for an exponentially structured, divergent stream. Let

$$v = V_B(1+\varepsilon_1 y)\exp\{-g(z)|x|\}\exp\times\left\{\ln\left[\frac{V_T(1+\varepsilon_3 y)}{V_B(1+\varepsilon_1 y)}\right]\left[\frac{z}{H}\right]\right\}, \quad (3.1)$$

$$g = g_0 \exp \mathrm{bz/H}. \quad (3.2)$$

The width of the stream at any z depends upon b. If $b>0$ ($b<0$), the stream is wider (narrower) at the ocean bottom than at the surface. The quantities $\varepsilon_1 y$, $\varepsilon_3 y$ parametrize divergence. Figure 11 is a schematic of this velocity structure for $b=0$. The requisite properties of the stream are calculated in terms of V_T, V_B and b,

$$C_1 = \frac{2f_0 V_B[2\ln(V_T/V_B)-b)\times 10^{10}}{H[V_T^2 e^{-b} - V_B^2]},$$

$$\frac{C_1}{C_2} = \frac{f_0 V_B[\ln(V_T/V_B)-b]\times 10^{-2}}{H\beta_0[V_T e^{-b} - V_B]}. \quad (3.3)$$

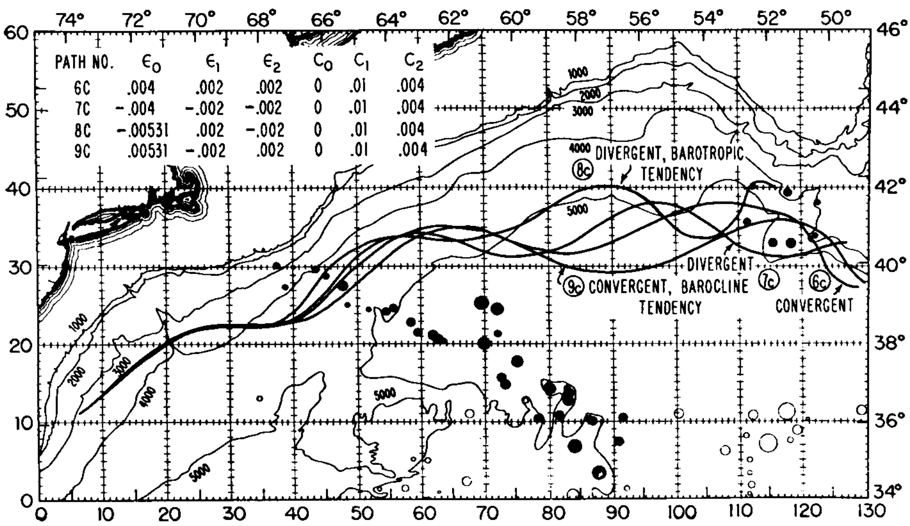

Fig. 10. Divergent–convergent stream paths over North Atlantic topography.

In the path equations, the divergent parameters $\varepsilon_0 y$, $\varepsilon_1 y$, $\varepsilon_2 y$ are linear in y, while expression (3.1) is not. In the range of interesting V_T, V_B, the integrals of expression (3.1) are smooth curves in y, which can be approximated by a straight line. Let $V_T(L)$, $V_B(L)$ be the values of surface and bottom velocities at the terminal of the solution curve $y = L$, whence the values of ε_i are calculated from

$$\varepsilon_0 \equiv \frac{1}{L}\left[\frac{\langle V^2(L)\rangle}{\langle V^2(0)\rangle} - 1\right]$$

$$= \frac{1}{L}\left\{\frac{[\ln(V_T/V_B) - b/2][V_T^2(L)e^{-b} - V_B^2(L)]}{[\ln(V_T(L)/V_B(L)) - b/2][V_T^2 e^{-b} - V_B^2]} - 1\right\}, \tag{3.4}$$

$$\varepsilon_1 \equiv \frac{1}{L}\left[\frac{\overline{V_B(L)}}{\overline{V_B(0)}} - 1\right] = \varepsilon_1. \tag{3.5}$$

$$\varepsilon_2 \equiv \frac{1}{L}\left[\frac{\langle V(L)\rangle}{\langle V(0)\rangle} - 1\right]$$

$$= \frac{1}{L}\left\{\frac{[\ln(V_T/V_B) - b][V_T(L)e^{-b} - V_B(L)]}{[\ln(V_T(L)/V_B(L)) - b]]V_T e^{-b} - V_B]} - 1\right\}, \tag{3.6}$$

$$\varepsilon_3 \equiv \frac{1}{L}\left[\frac{V_T(L)}{V_T(0)} - 1\right] = \varepsilon_3. \tag{3.7}$$

In solution paths $6C$–$9C$ a power series development in $\varepsilon_i y$ of (3.4) and (3.6) was used to evaluate ε_0, ε_2. In solution paths in section 5 the actual values of ε_0, ε_2 calculated from (3.4) and (3.6) were used in the integrating routine. Figure 13 is the plot of V_T vs. V_B for constant values of C_1 and C_1/C_2. The values $f_0 = 0.935 \times 10^{-4}$, $\beta_0 = 1.75 \times 10^{-13}$, $H = 4 \times 19^5$ (c.g.s.) were used.

Table 2. *Percentage changes of divergent stream properties*

Solution path	Top velocity change, %	Bottom velocity change, %	Transport change, %	Tendency
6C	+30	+30	+30	Pure convergent
7C	−30	−30	−30	Pure divergent
8C	−55	+30	−30	Divergent, Barotropic
9C	+55	−30	+30	Convergent, Baroclinic

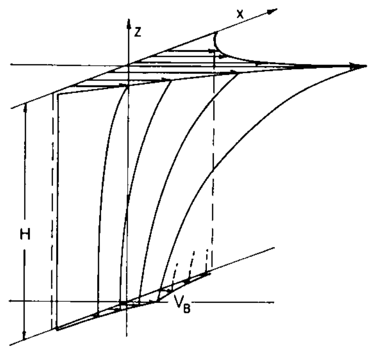

Fig. 11. Schematic velocity profile for exponentially structured stream.

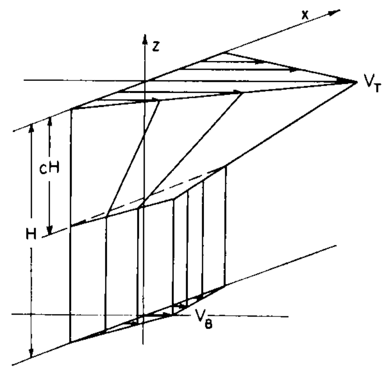

Fig. 12. Schematic velocity profile for polygonally structured stream.

3.2. *The polygonal model*

Figure 12 is the schematic of the polygonal model of the velocity structure. In terms of this model C_1 and C_2 are

$$C_1 = \frac{3}{2}\frac{f_0 V_B}{H}\left\{\frac{10^{10}}{V_B^2[1-c]+cV_BV_T+\frac{1}{3}c[V_T-V_B]^2}\right\}, \tag{3.8}$$

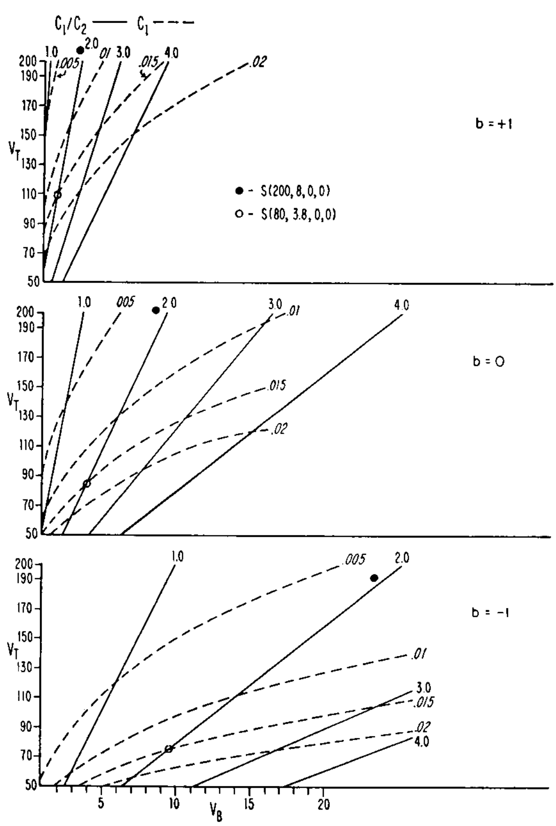

Fig. 13. Values of C_1 and C_1/C_2 as function of top and bottom velocity of an exponentially structured stream.

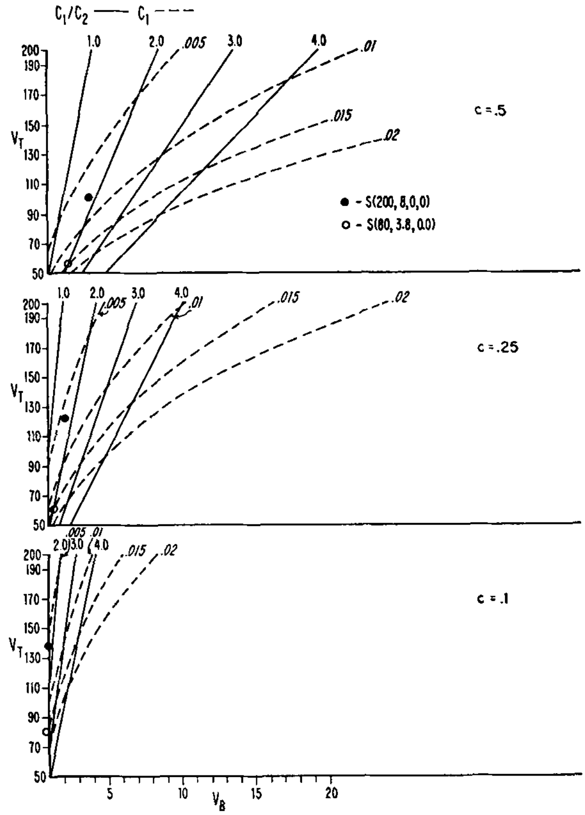

Fig. 14. Values of C_1 and C_1/C_2 as function of top and bottom velocity of a polygonally structured stream.

$$(C_1/C_2) = \frac{f_0 10^{-2}}{H\beta_0} \left\{ \frac{V_B}{V_B + c/2(V_T - V_B)} \right\}. \qquad (3.9)$$

Figure 14 is the plot of V_T vs. V_B for fixed values of C_1 and C_1/C_2.

4. The observed paths

The data available on actual Gulf Stream paths through 1960 has been summarized and discussed by Warren (1963 § 1). Subsequent data consist of several paths obtained by the tracking of the 15°C isotherm at 200 m by the use of a continuously recording towed thermistor and of bathythermographs. Three such paths were obtained in 1964 by Fuglister & Voorhis (1964). Since September of 1965 the Coast and Geodetic Survey has traced that isotherm monthly (the ESSA-paths). Figure 15 is a composite of all available paths including 9 preliminary ESSA-paths through May 1966.

Interpretation of the 15°C isotherm data is moot, particularly because of the time variability apparent in the ESSA data, and because of the uncertainty of the identification of the isotherm trace with the stream axis as defined in the vertically coherent quasi-steady theory. Nonetheless, comparison will be made between the data of Figure 15 and numerically calculated paths.

To quantify the comparison, three gross statistical features of the paths were chosen to characterize (i) the position, (ii) the shape of the envelope of paths and (iii) the average scale or wavelength of the meanders. In the ensuing analysis the zeros of curvature of the paths play an important role. Two simple processes for filtering small scale detail were adopted by disregarding zeros of curvature which were not separated by at least one degree of longitude (wavelength filter) and by disregarding meanders which had an amplitude of less than one-

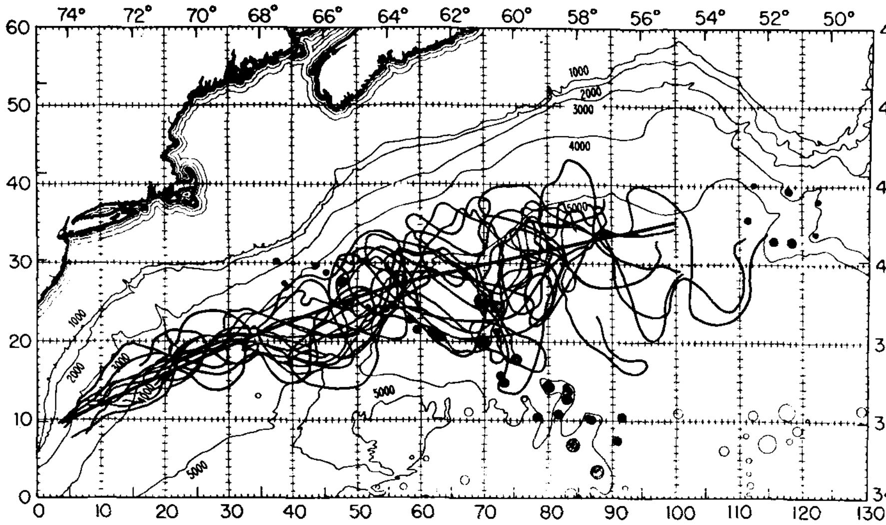

Fig. 15. Composite of all available Gulf Stream paths through May 1966.

half degree of latitude about the mean position (amplitude filter).

The mean position (i) is adequately described by the control curve as defined. The heavy line on Figure 15 is the control curve constructed from the ESSA data (see Fig. 16) by mapping the seros of curvature from all 9 paths and passing a smooth line downstream through the center of mass of the distribution. Upon superposition of this curve on the earlier data it was decided to regard this curve simply as the observed control curve for all paths. The envelope property (ii) was not defined rigorously and comparison will be made amply by eye; e.g. east of 63° the paths lie generally between the latitudes 38 to 42° N.

As a measure of the average wave-length (iii) the quantity N = *number of zeros of curvature per degree of longitude was defined.* This is convenient because of the variety of lengths and locations of the observed path segments. Averages of N over the data were calculated as displayed in the first two lines of Table 3.

The monthly deviations of the ESSA paths

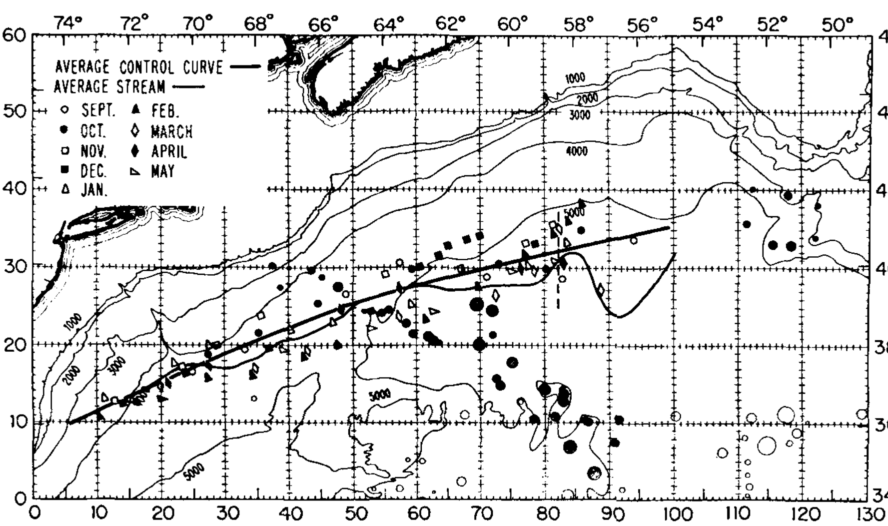

Fig. 16. Control curve and zeros of curvature from ESSA paths.

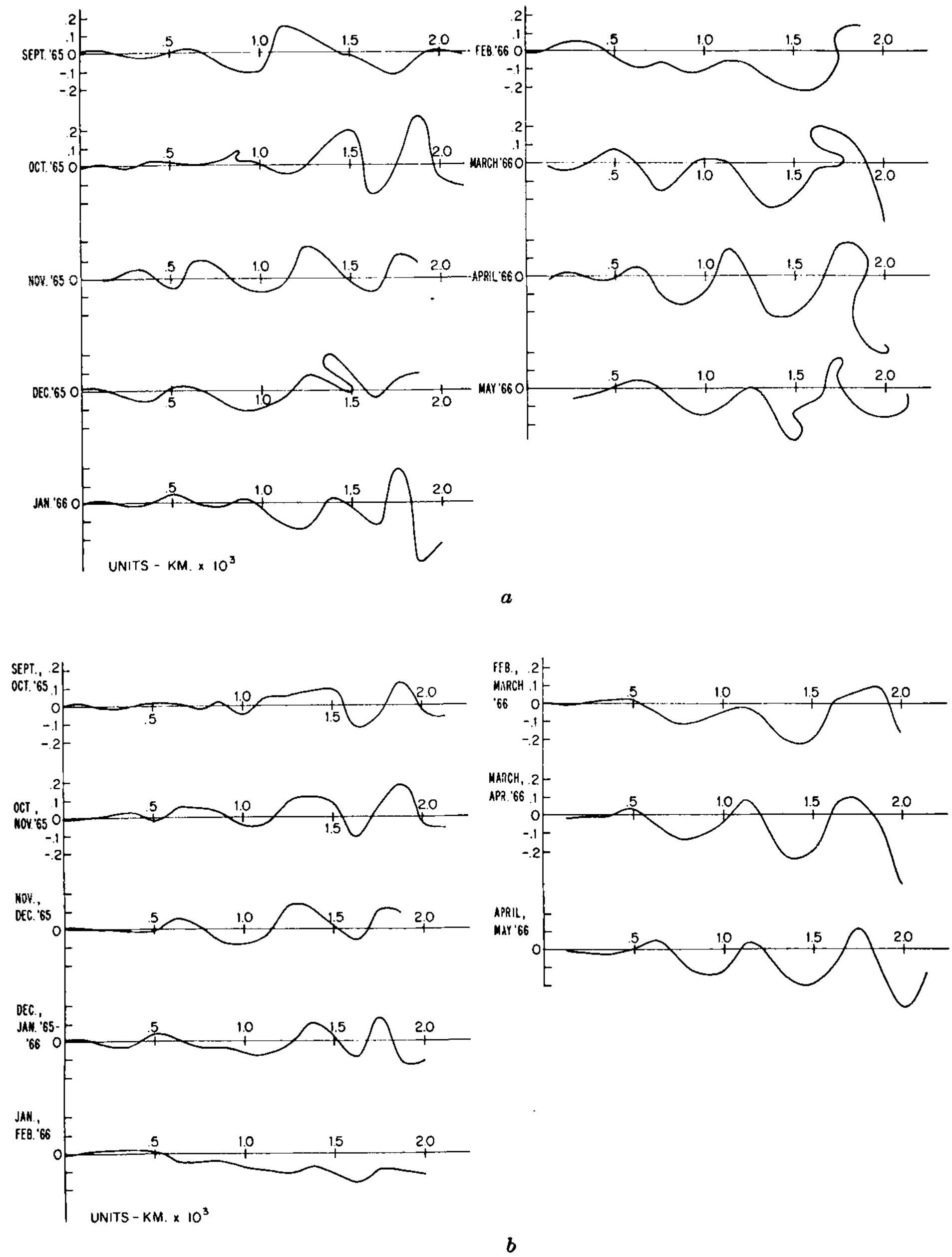

Fig. 17 (*a*) Monthly deviation of ESSA paths from the control curve. (*b*) Bi-monthly average deviation of ESSA paths from the control curve.

from the observed control curve are plotted in Figure 17*a*. Little regularity is apparent, but more appears in Figure 17*b*, which is the bimonthly average of the monthly deviations. The bimonthly averages were constructed with the idea of possibly revealing the semi-permanent or quasi-steady features of the meanders, i.e. by an averaging out of the more rapidly varying features. Tri-monthly averages were constructed and did not differ significantly

Table 3. *Summary of N, the count of zeros of curvature per degree longitude*

	Wavelength filter	Wavelength and amplitude filter
Gulf Stream data before Sept. '65	.54	.36
ESSA data. Monthly deviation	.41	.34
ESSA data. Bi-monthly deviation	.36	.30
S(200, 8, 0, 0)	.21	
S(80, 3.8, 0, 0)	.41	
S(200, 8, 0.50, 0.65)	.28	
S(150, 7, 0.85, 0)	.34	

from the bi-monthly. Averaging over longer and longer times, of course, changes the picture entirely as can be seen from the average path over 9 months shown on Figure 16. The average value of N for the bi-monthly curves is given in line 3 of Table 3. It is significantly lower than the N values for the raw data.

5. The numerical experiment

The design of the numerical experiment was guided by the quality and the nature of the available data and the degree of sophistication of the mathematical model. For an assumed model stream (or coefficient parameter set P: $(C_1, C_2, \varepsilon_0, \varepsilon_1, \varepsilon_2)$) many solutions were obtained for a variety of initial conditions ($Y(0)$, $Y'(0)$, C_0). The numerical statistics thus produced were then compared with the three properties defined in the last section. Small changes in the choice of $Y(0)$ were early seen not to affect the statistics and such variations were dropped.

The choice of model stream considered was motivated in two ways: by the available velocity data on the Gulf Stream and by the search for the range of P which reproduced statistical features of the observed stream. In the first instance, a model stream and a stream parameter set S: $(V_T, V_B, \varepsilon_1 L, \varepsilon_2 L)$ was chosen and P computed; in the latter instance, S was inferred from P. In the definition of S an average L of 2550 km may be understood.

A summary of the experiments performed is given in Figure 18*a* and 18*b* on which a filled circle denotes a non-divergent experiment and an arrow beginning with a star and ending in a circle denotes a divergent experiment. The shaft of the arrow represents the sequence of effective C_1, C_2 values pertinent to the solutions if regarded as "quasi-non-divergent"; i.e., the tail of the arrow lies at C_1, C_2 and the point lies at $C_1\,(1+\varepsilon_1 L)\,(1+\varepsilon_0 L)^{-1}$, $C_2\,(1+\varepsilon_2 L)(1+\varepsilon_0 L)^{-1}$.

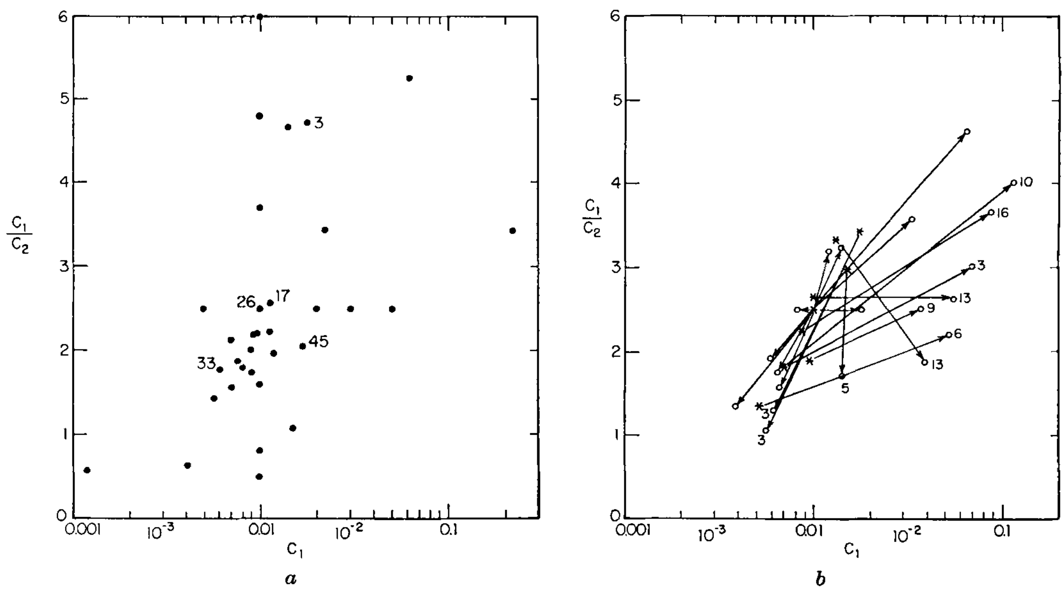

Fig. 18. (*a*) Summary of numerical experiments; non-divergent stream. (*b*) Summary of numerical experiments; divergent stream.

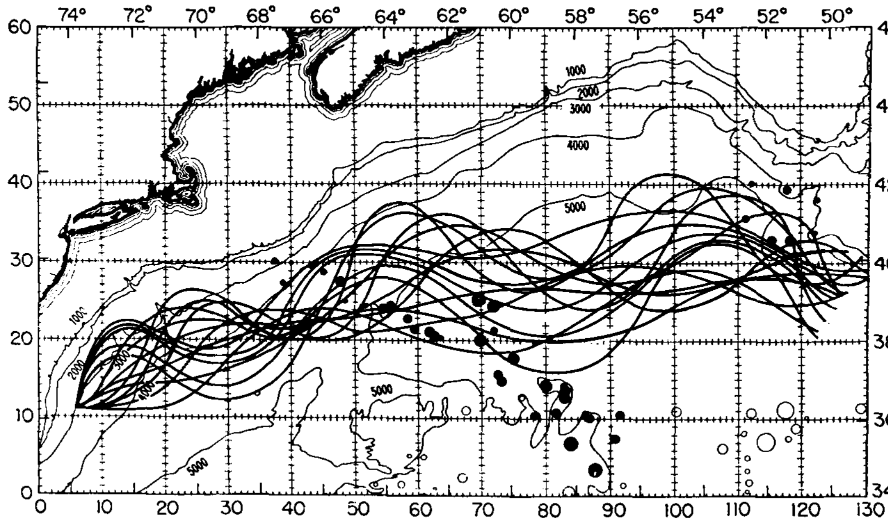

Fig. 19. Composite of solution paths $S(200, 8, 0, 0)$.

To interpret these experiments oceanographically, the filled circles and arrows may be referred to the diagram of Figures 13, 14, 23, upon which a few are actually displayed. It was decided to investigate only simple and smooth profile shapes, and under that condition the simple exponential and polygonal models of section 3 were found to be sufficiently general. The vertical shape characteristics are described by baroclinicity parameters (the polygonal constant-c and the exponential factor in (V_T/V_B)) and a parameter descriptive of the depth dependence of horizontal decay (the exponential constant-b). Calculations were made for other shapes, but yielded nothing of qualitative interest. It should be noted that, since the coefficients depend only upon ratios of integrals, they are independent of the width of the jet. In particular, if a gaussian structure in the horizontal direction is assumed, very little difference results from the exponential model. A "champagne glass" structure of the stream as proposed by Knauss (1966) gives results similar to an exponential model with $b > 0$. The schematic

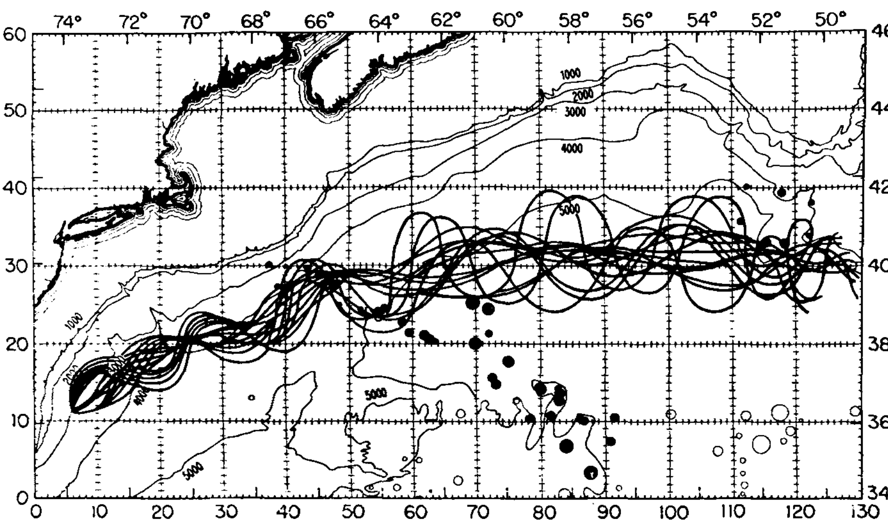

Fig. 20. Composite of solution paths $S(80, 3.8, 0, 0)$.

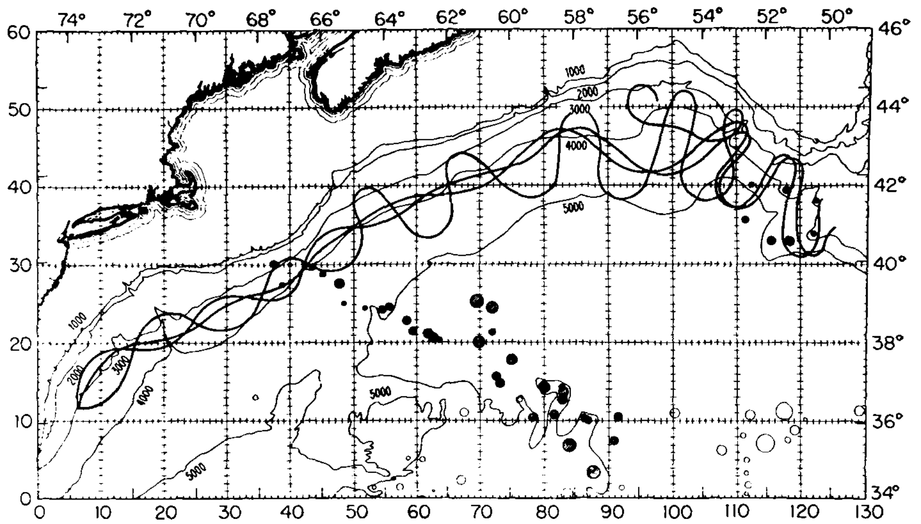

Fig. 21. Solutions of Warren's choice of top and bottom velocities $S(160, 10, 0, 0)$.

velocity structure proposed for the stream by Fuglister & Voorhis (1964, Fig. 1) yields values of $C_1 = 0.0081$, $C_1/C_2 = 3.7$. Warren's (1963) calculations were made on the polygonal model with $C = 1/4$, $V_T = 160$, $V_B = 16$; his values of V_T, V_B in the exponential model correspond to $C_1 = 0.014$, $C_1/C_2 = 4.7$.

In general it was found that with reasonable values of V_T, V_B the steady state model could reproduce the observed control curve and envelope spread, but that the meander wavelengths were too long when compared to the raw data; i.e., the N-values were significantly smaller than those of Table 3, column 1, lines 1 and 2.

Consider first the non-divergent cases. On Figures 20 and 21 are plotted composites of paths for the combinations of initial conditions $Y_0' = 0$, 0.57, ∞, $C_0 = 0$, ± 0.04. The choice of $S(200, 8, 0, 0)$ (Fig. 20) is consistent with known velocity measurements on the Gulf Stream, including Knauss' (1966) bottom velocity data; the choice of $S:(80, 3.8, 0, 0)$ (Fig. 20) is the best non-divergent fit obtained to the observed statistics. (Here and hereafter S values refer to an exponential model with b = 0 unless specifically stated otherwise.) The respective N values are 0.21 and 0.41 (a slightly higher N value could easily have been achieved, but this was not considered worthwhile). In both cases the control curve agrees with the observed one. The initial shape of the envelope near Cape Hatteras, which is thicker than observed on Figures 19 and 20, can easily be changed by manipulation of the initial conditions without change of calculated statistics.

Qualitatively identical results obtain to all simple stream structures investigated, as may be seen from Figures 13 and 14, by noting the relative position of the observational points $S:(200, 8, 0, 0)$ and the best fit points given by the intersection of the curves of $C_1 = 0.015$ and $C_1/C_2 = 2$. The best fit points are summarized in Table 4.

As anticipated in the discussion of section 2, for the range of coefficients explored the wavelength was controlled essentially by C_1, and the control curve by C_1/C_2. On Figure 21 are shown three typical paths for Warren's choice of top and bottom velocities, $S:(160, 10, 0, 0)$. The wavelength agreement is good ($N = 0.42$), but the control curve is not. With $C_1/C_2 = 4.7$ the solution paths do not fall from the initial isobath down onto the abyssal plain. Thus it must be

Table 4. *Summary of best fit points for non-divergent experiments*

Velocities in cm/sec

Exponential model						Polygonal model					
$b = +1$		$b = 0$		$b = -1$		$c = 0.5$		$c = 0.25$		$c = 0.1$	
V_T	V_B	V_T	V_B	V_T	V_B	V_T	V_B	V_T	V_B	V_T	V_B
110	2	80	3.8	79	9.5	58	2.2	60	1.6	81	.8

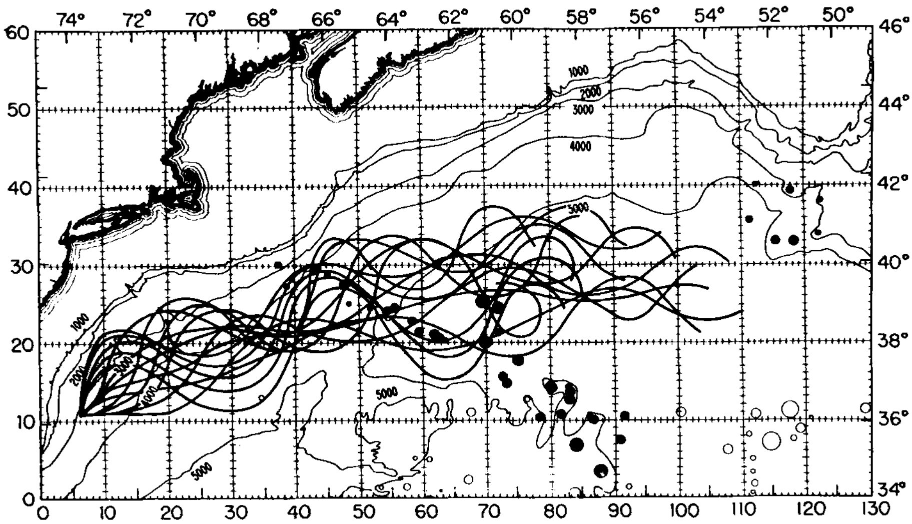

Fig. 22. Composite of solution paths $S(200, 8, 0.50, 0.60)$.

concluded that the steady state non-divergent theory cannot account for the details of individual Gulf Stream paths, in contradistinction to Warren's conclusion. In the comparison of our results with Warren's it is important to note that it is *not* the details of the topography which steer the stream down the Continental Rise, but, rather, *the ratio of the β-effect to the topography effect*. Although the β-effect is apparently small over any meander, it is cumulative.

The result that the control curve can be deduced correctly from the steady state theory while the detailed meanders cannot may be geophysically meaningful. If the time dependence is assumed to be slow and the transient stream assumed to remain always coherent, the time dependent generalization of the $\varkappa$-equation has been obtained (Niiler, 1966). The control curve equation which results from the time average of that equation is identical to eq. (2.1).

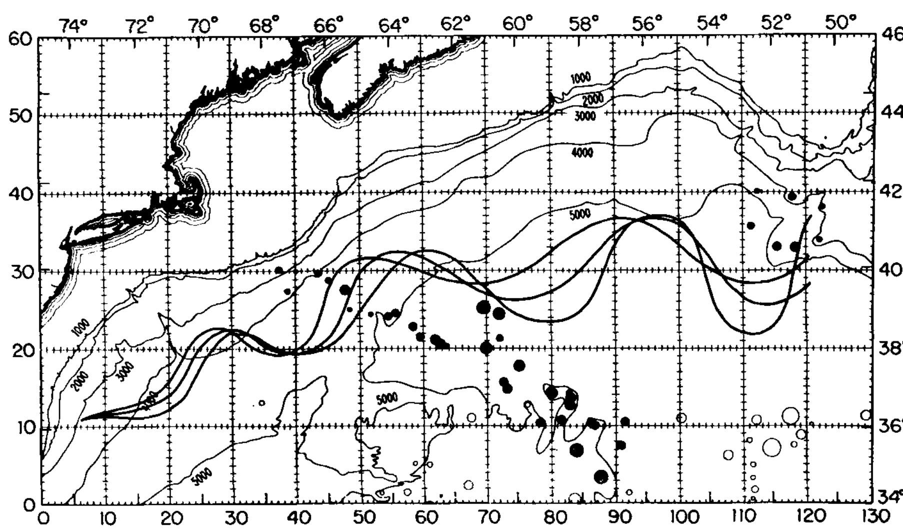

Fig. 23. Solution path with a divergent, baroclinic tendency $S(150, 7, 0.85, 0)$.

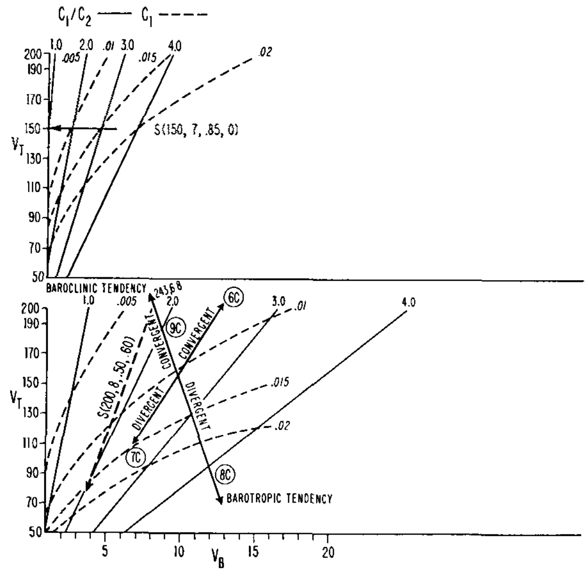

Fig. 24. Location of divergent experiment paths on V_T, V_B diagram.

The surface velocity of the Gulf Stream is known to decrease from Cape Hatteras to the Grand Banks (although nothing is known of the bottom velocity). Thus a better fit to the observational statistics may be expected from divergent calculations, since Table 4 favours low values of V_T. Also the envelope shape may be improved if the (ad hoc) assumption of barotropic tendency is made, and adjusted to dominate the amplitude effect while the divergence dominates the wavelengths. A result of interest is shown in Figure 22, for S: (200, 8, 0.50, 0.60) which corresponds to $V_T(L) = 80$, $V_B(L) = 4$; $N = 0.28$. In an attempt to improve the N-comparison a bias of negative curvature ($C_0 < 0$) in the initial conditions was used to obtain reasonable control curves for higher C_1/C_2 values. The best of these is shown on Figure 23, for which S: (150, 6, 0.85, 0) on a $b = 1$ exponential model and $N = 0.34$.

A summary comparison between the theoretical and observational N values is made on the observed N, Table 3. It must be concluded that the detail of the 200 m 15° isotherm trace cannot be accounted for on a steady state meander theory of this type. The relevance of the good aggreement with the bi-monthly average data and the doubly filtered data is offered to the readers' judgement. The question of the existence and nature of quasi-permanent larger scale features of the paths awaits further investigation—both observational and theoretical.

Acknowledgements

We wish to thank Dr. Donald Hansen for his kindness in making available the preliminary results of the ESSA cruises. Miss Patricia Jaskun's valued assistance in the programming, calculations, and preparation of figures is gratefully acknowledged. This research was supported by the Office of Naval Research under Contract NR-083-201 to Harvard University.

REFERENCES

Fuglister, F. C. & Voorhis, A. D. 1966. *A new method of tracking the Gulf Stream.*

Knauss, J. 1966. Private communication.

Niiler, P. P. 1966. Theory of free inertial jets on a rotating globe. Proceedings of the 5th Natl. Congress of Applied Mechanics, pp. 722–730.

Pratt, R. 1965. Private communication.

Robinson, A. R. & Niiler, P. P. 1967. Theory of free inertial jets, I. Path and structure. *Tellus 19*, 2.

Warren, B. A. 1963. Topographical influences on the path of the Gulf Stream. *Tellus 15*, 2, pp. 167–183.

ТЕОРИЯ СВОБОДНЫХ ИНЕРЦИОННЫХ СТРУЙ: II. ЧИСЛЕННЫЙ ЭКСПЕРИМЕНТ, МОДЕЛИРУЮЩИЙ ПУТЬ ГОЛЬФСТРИМА

Получены численные решения уравления пути свободной струи, которое было выведено в первой части этого исследования, при значениях параметров, соответствующих Гольфстриму. Проведено сравнение с данными наблюдений. Показано, что такая стационарная теория может описывать среднее положение течения при его падении с континентального шельфа в глубокую воду. Обсуждаются некоторые детали меандрирования течения относительно среднего положения.